$(\sqrt{13}\times\sqrt{13})R13.9°$ and $(\sqrt{7}\times\sqrt{7})R19.1°$ reconstructions of the polar $SrTiO_3$ (111) surface

Bruce C. Russell and Martin R. Castell*
Department of Materials, University of Oxford, Parks Road, Oxford, OX1 3PH, United Kingdom
(Received 27 July 2006; revised manuscript received 23 January 2007; published 27 April 2007)

Nb-doped $SrTiO_3$ (111) samples are annealed in UHV at 850 °C for 30 min and investigated using scanning tunneling microscopy (STM), low-energy electron diffraction (LEED), and Auger electron spectroscopy (AES). STM images show that both $(\sqrt{7}\times\sqrt{7})R19.1°$ and $(\sqrt{13}\times\sqrt{13})R13.9°$ reconstructions coexist on the surface. Step heights of 0.21 ± 0.02 nm on the surface are equivalent to the d_{111} lattice parameter, which is the distance between two adjacent, similar (111) planes in the bulk crystal. The calculated LEED pattern for this co-reconstruction corresponds to the observed LEED pattern, which resembles a six-petal flower. AES analysis indicates no detectable impurities, and shows the surface to be Ti and Sr enriched and O deficient compared to the bulk stoichiometry. This change in surface composition is proposed to provide the stability for the polar surface.

DOI: 10.1103/PhysRevB.75.155433 PACS number(s): 68.47.Gh, 68.35.Bs, 68.37.Ef, 61.14.Hg

I. INTRODUCTION

Polar surfaces of ionically bonded materials are of great interest because no charge-neutral bulk termination exists. A bulk-terminated surface is the arrangement the atoms would have if a cut were made through the bulk of the solid, and the atoms were prevented from moving from their positions. Tasker[1] predicted that the stability of a surface depends upon the overall charge distribution, perpendicular to the surface, within the bulk of the material. If a perpendicular macroscopic dipole is present, the surface energy is infinite, and hence the termination is unstable. If no dipole is present, the surface energy has a finite value, but may still be very large. We thus define a polar surface as an interface where, if a bulk termination were to be adopted, a dipole would be present throughout the crystal, causing an infinite surface energy.

In order for a polar surface to exist it must be possible to remove the dipole.[2] The main four mechanisms are changing the surface stoichiometry, redistribution of electrons in the surface region, adsorption of atoms or molecules, and faceting. If the surface layers become nonstoichiometric, a different phase will be produced in the first few layers of the surface. The charge distribution at the surface will, hence, be different from a bulk termination, and this can quench the dipole. If the surface phase is ordered, a reconstruction is produced. The second mechanism is when the stoichiometry is preserved, and the removal of the polarity is due to a redistribution of the electronic charge within the surface region as a response to the polar electrostatic field. This change in the charge density in the surface region removes the dipole. In the third mechanism, atoms or molecules are adsorbed from the residual atmosphere. This in turn can cancel the dipole. If none of these methods lowers the energy sufficiently, microfaceting may occur, as the increase in surface area is usually easily compensated by the vastly reduced surface energy of nonpolar facets.

In oxide crystals the constituent atoms are nominally charged; the metal forming positively charged cations, and the oxygen negatively charged anions. The crystal can be considered as made up of repeating layers of ions, parallel to the surface termination of interest. Depending upon the crystallographic orientation of the surface, these layers may possess a charge and hence form a polar termination. An example is the $SrTiO_3$ (111) surface. $SrTiO_3$ crystallizes into a cubic perovskite structure with a 0.3905 nm lattice parameter, and formal ionic charges of Sr^{2+}, Ti^{4+}, and O^{2-}. The Ti ions are six-fold octahedrally coordinated with respect to the O ions, and the Sr ions are in a site that is 12-fold coordinated by O ions. The perovskite unit cell is shown in Fig. 1(a) with a SrO_3^{4-} (111) plane indicated in gray. $SrTiO_3$ viewed in the $\langle 111\rangle$ directions is made up from a stack of alternating charged Ti^{4+} and SrO_3^{4-} planes as shown in Fig. 1(b). The distance between two adjacent similar planes (e.g., two SrO_3 planes) is known as the d_{111} lattice spacing, and has a magnitude of 0.23 nm. In $SrTiO_3$ (111) the alternating positive Ti^{4+} and negative SrO_3^{4-} charged (111) planes lead to the polar nature of this surface.

Pure $SrTiO_3$ is a clear colorless crystal with a high refractive index. $SrTiO_3$ has applications as a substrate for the growth of high-T_c superconducting films,[3] surface photoelectrolysis,[4] surface chemical reactions,[5] and oxygen gas sensing.[6] $SrTiO_3$ (100) has also been used for the epitaxial growth of metal nanocrystals,[7,8] and the different surface

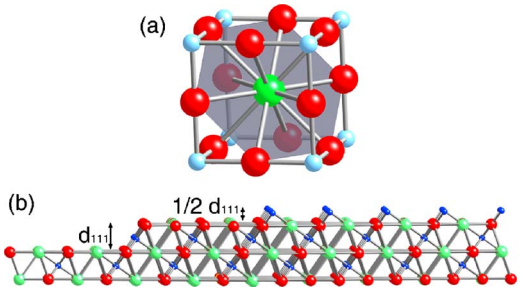

FIG. 1. (Color online) (a) Unit cell of $SrTiO_3$ with the SrO_3^{4-} (111) plane indicated. Sr ions at the center of the unit cell are green (medium gray), Ti ions, which are situated at the corners of the unit cell, are blue (light gray). O ions are red (dark gray) and are found at the center of the edges of the unit cell. (b) Bulk-terminated $SrTiO_3$ (111) surface viewed from the side. The material is made up of alternating Ti^{4+} and SrO_3^{4-} layers. A step is shown from a Ti-terminated layer to a SrO_3-terminated layer ($1/2\ d_{111}$) and between two SrO_3 layers (d_{111}).

reconstructions have been shown to favor different crystal shapes.[9] The characterization of the surfaces of $SrTiO_3$ is thus of great interest for the improvement of these applications.

Unlike the $SrTiO_3$ (100) surface where a number of reconstructions.[10–13] and surface nanostructures[14–16] have been observed, there is a limited amount of data available about the $SrTiO_3$ (111) surface. Lo and Somorjai[17] showed that surfaces sputtered at 600 °C in UHV exhibited irreversible faceting and were Sr enriched, while those sputtered at room temperature in UHV exhibited a flat (1×1) surface, which suffered a decrease in the Sr concentration when heated in UHV to 600 °C.

One of the few reported reconstructions is a Ti^{4+}-rich (4×4) reconstruction produced by Haruyama *et al.*[18] after annealing in UHV at 1200 °C for 5 min. This periodicity was observed in low-energy electron diffraction (LEED), and scanning tunneling microscopy (STM) images have so far not been published. They also reported a (1×1) surface after annealing for 1 h at 800 °C in UHV.

STM data on the surface are sparse. Tanaka and Kawai[19] indicated that samples annealed in UHV at 1180 and 1220 °C both contained step heights of integer multiples of the d_{111} lattice spacing and, in contrast, the intermediate condition of 1200 °C exhibited step heights of integer multiples of $\frac{1}{2}d_{111}$ (which is the distance between two adjacent, dissimilar SrO_3 and Ti layers in the bulk). The 1180 °C annealed sample gave images of a smooth surface, whereas the 1220 °C sample was more granular. In reflection high-energy electron diffraction both surfaces exhibited the same (1×1) periodicity, but the 1180 °C sample also had extra streaks, which were of unclear origin. Later studies by Sigmund *et al.*[20] suggest samples annealed in a UHV chamber at 950 °C for 2 h have step heights equivalent to the d_{111} lattice spacing.

Atomic force microscopy (AFM) has also been used to investigate the effect of annealing for 10 h at 1000 °C in different gases, all at a pressure of 1 atm.[21,22] The Ar-annealed surface contained large flat triangular terraces and had step heights of multiples of $\frac{1}{2}d_{111}$, whereas the oxygen-annealed surface had a trench structure, with step heights equivalent to d_{111}, and an increase in the Ti:Sr ratio in comparison to the Ar-annealed sample. The air-annealed structure produced AFM images resembling a fractal shape called Sierpinski's gasket,[23] containing many triangular facets of different sizes.

In this paper we present high-resolution STM images of a $SrTiO_3$ (111) reconstruction, allowing individual unit cells to be seen, and answer the question of whether the step heights are integer multiples of d_{111} or $\frac{1}{2}d_{111}$.

II. EXPERIMENT

$SrTiO_3$ single crystals doped with Nb at 0.5 wt % with epi-polished (111) surfaces were supplied by PI-KEM, U.K. Electronically, $SrTiO_3$ is an insulator as it has a band gap of 3.2 eV at 25 °C.[24] Nb dopes $SrTiO_3$ *n*-type, giving rise to good electrical conduction at room temperature. The crystals were introduced without pre-treatment into the ultrahigh vacuum chambers of two instruments. The first was a JEOL JSTM4500xt which includes STM and LEED analysis facilities. The second instrument was a JEOL JSTM4500s comprising STM, LEED, and a UHV scanning electron microscope with a SPECS PHOIBOS 100 electron energy analyzer. The latter two instruments can be used in combination to provide Auger electron spectroscopy (AES) at high spatial resolution. Both instruments are also equipped with ion sputtering facilities. The vacuum on each instrument was regularly observed to be of the order of 10^{-8} Pa. Etched tungsten tips were used in the STM to provide constant-current images at room temperature. Sample annealing was achieved by resistively passing a direct current through the sample and the temperatures were measured through a viewport with an optical pyrometer.

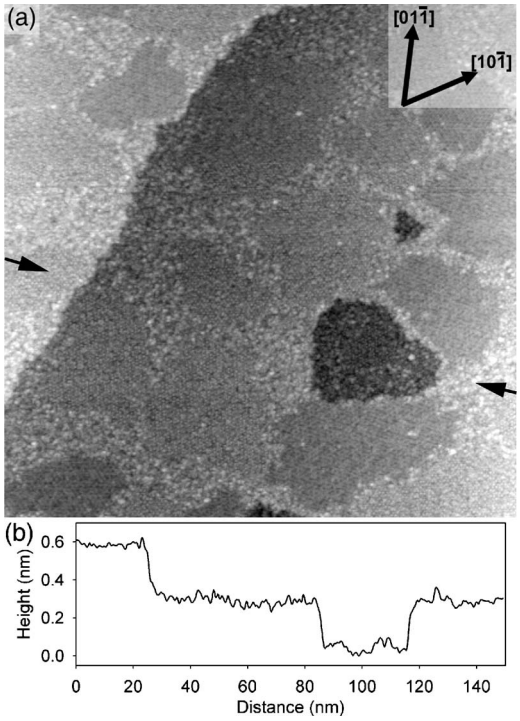

FIG. 2. (a) Image showing domains of the $(\sqrt{13}\times\sqrt{13})R13.9°$ and $(\sqrt{7}\times\sqrt{7})R19.1°$ reconstructions and irregularly shaped step edges. Disorder can be seen between the reconstructed domains (image size 150×150 nm^2, sample bias +2.0 V, tunneling current 0.2 nA). (b) Topography trace of the image in (a) in a straight line between the two arrows. Step heights are equal to the d_{111} lattice parameter (0.23 nm).

III. RESULTS

A. Scanning tunneling microscopy

A $SrTiO_3$ crystal with a (111) polished surface was introduced into the chamber and annealed in UHV at 850 °C for 30 min. After annealing, the surface was observed using the STM as shown in Fig. 2. The image is a 150×150 nm^2 scan of the surface containing a number of ordered domains. Terraces separated by step edges can also be seen. The STM

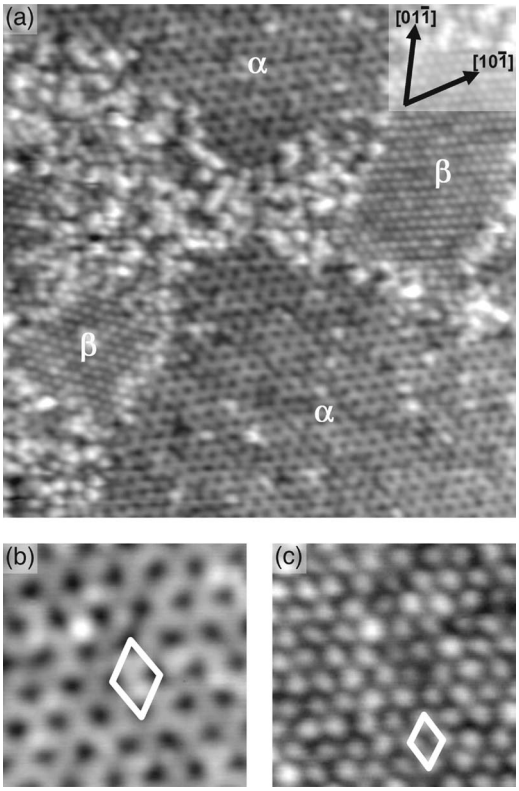

FIG. 3. (a) Domains toward the top and bottom (α) are $(\sqrt{13}\times\sqrt{13})R13.9°$, and those at the right- and left-hand sides (β) are $(\sqrt{7}\times\sqrt{7})R19.1°$. The two β regions show two different rotational domains, whereas the α regions show the same rotation from the underlying bulk lattice (image size 65×65 nm^2, sample bias +2.9 V, tunneling current 0.3 nA). (b) Image of the $(\sqrt{13}\times\sqrt{13})R13.9°$ reconstruction with the unit cell indicated (image size 12×12 nm^2, sample bias +3.6 V, tunneling current 0.12 nA). (c) Image of the $(\sqrt{7}\times\sqrt{7})R19.1°$ reconstruction with the unit cell indicated (image size 12×12 nm^2, sample bias +2.14 V, tunneling current 0.1 nA).

images indicate that the step edges are jagged and do not follow any particular crystallographic direction. The pit in the bottom right has a step edge surrounding it with no obvious straight facets. While a large amount of the surface appears to be covered in ordered domains, there is still a significant amount of disorder present. Boundaries between domains tend to be disordered. The step heights have a magnitude of 0.21 ± 0.02 nm which is equivalent to the d_{111} lattice parameter of 0.23 nm [the distance between two adjacent, similar (111) layers in the bulk]. Figure 2(b) shows a height profile for a straight line between the two black arrows. The step edges are equivalent to the d_{111} lattice parameter.

A higher-resolution image of the surface is shown in Fig. 3(a), where one can see two different reconstructions. The two large domains to the top and bottom of the image (α) have a larger periodicity than the two smaller domains to the left and right of the image (β). The β domains are also somewhat different from one another. On closer inspection it can be seen that they are rotational domains of one another. On comparison with other images, rotational domains were also observed for the α domains. The periodicity of the β domains was measured to be 1.46 ± 0.07 nm while that of the α domains was found to be 1.99 ± 0.09 nm. The underlying $SrTiO_3$ (111) (1×1) bulk termination has a periodicity of 0.55 nm. Reconstructions are described by the multiple of their periodicity compared to that of the bulk-terminated surface. Thus, when compared with the underlying $SrTiO_3$ (111) (1×1) lattice, the periodicities of the α and β domains are ~3.5 and ~2.5, respectively, as a multiple of the bulk lattice. These values, and the presence of rotational domains in both structures, mean that the reconstructed unit cells must be rotated with respect to the underlying bulk unit cell, and that the periodicities are noninteger. Two structures that satisfy these conditions, and have periodicities similar to those in the images, are the $(\sqrt{13}\times\sqrt{13})R13.9°$ (with a unit cell periodicity of 1.99 nm) and $(\sqrt{7}\times\sqrt{7})R19.1°$ (with a unit cell periodicity of 1.46 nm) reconstructions.

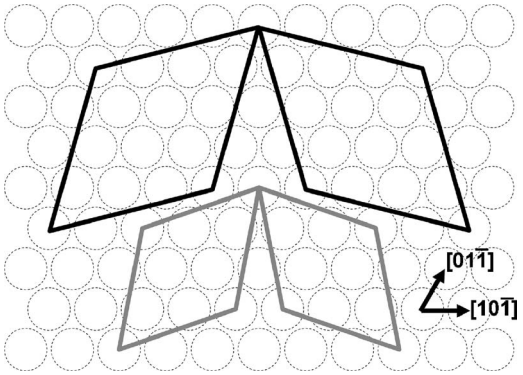

FIG. 4. Illustration of the unit cells of the two rotational domains of the $(\sqrt{7}\times\sqrt{7})R19.1°$ (gray) and $(\sqrt{13}\times\sqrt{13})R13.9°$ (black) reconstructions.

We thus assign the $(\sqrt{13}\times\sqrt{13})R13.9°$ to the α domain reconstructions at the top and bottom of Fig. 3(a) and the $(\sqrt{7}\times\sqrt{7})R19.1°$ to the β domains on the left and right. Figure 3(b) shows a highly magnified region of the $(\sqrt{13}\times\sqrt{13})R13.9°$ reconstruction. It is characteristically imaged at sample biases around +3.6 V. The $(\sqrt{13}\times\sqrt{13})R13.9°$ images contain dark spots on a lighter background. Figure 3(c) is an image of the $(\sqrt{7}\times\sqrt{7})R19.1°$ reconstruction, which in contrast to the $(\sqrt{13}\times\sqrt{13})R13.9°$ surface has bright spots on a darker background. Figure 4 shows the two rotational domains of the $(\sqrt{7}\times\sqrt{7})R19.1°$ (indicated in gray) and the two rotational domains of the $(\sqrt{13}\times\sqrt{13})R13.9°$(in black).

B. Low-energy electron diffraction

The coexisting reconstructions observed using STM were probed further using LEED. Figure 5(d) shows the LEED pattern obtained for our $(\sqrt{13}\times\sqrt{13})R13.9°$ and $(\sqrt{7}\times\sqrt{7})R19.1°$ reconstructed samples, taken at an electron energy of 51 eV. The integer-order spots are most intense, and with their typical hexagonal pattern, they are clearly visible. There are also a number of noninteger spots. These are present as a pattern of arcs between the integer order spots. Each arc comprises six spots. The overall effect is for each

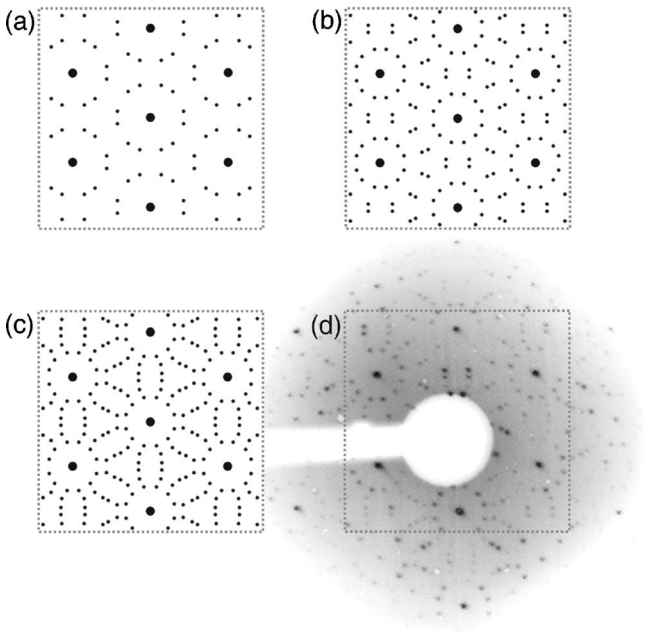

FIG. 5. Generic and observed LEED patterns for the $(\sqrt{7}\times\sqrt{7})R19.1°$ and $(\sqrt{13}\times\sqrt{13})R13.9°$ reconstructions. All calculated patterns were obtained using LEEDPAT (Ref. 27). (a) Calculated generic LEED pattern for the two rotational domains of a $(\sqrt{7}\times\sqrt{7})R19.1°$ reconstruction. (b) Generic LEED pattern of the two rotational domains of a $(\sqrt{13}\times\sqrt{13})R13.9°$ reconstruction. (c) Superposition of the calculated generic LEED patterns of coexisting $(\sqrt{7}\times\sqrt{7})R19.1°$ and $(\sqrt{13}\times\sqrt{13})R13.9°$ reconstructions. (d) Observed LEED pattern for the annealed surface. The gray scale of the LEED pattern has been inverted (electron energy 51 eV). This pattern is the same as in (c).

pair of arcs to resemble a petal on a flower, with an integer order spot at the center.

In order to confirm our hypothesis about the surface structure, we calculated the generic LEED patterns for both the $(\sqrt{13}\times\sqrt{13})R13.9°$ and the $(\sqrt{7}\times\sqrt{7})R19.1°$ reconstructions using the LEEDPAT software package.[27]

The pattern for a surface with $(\sqrt{7}\times\sqrt{7})R19.1°$ periodicity is shown in Fig. 5(a). Two rotated $(\sqrt{7}\times\sqrt{7})R19.1°$ domains are possible and, since these domains have the same probability of existing, they are present in equal quantities. Thus the spots for each domain are similarly intense. Each domain leads to a separate LEED pattern with six noninteger spots around the integer spots. These two-domain LEED patterns are themselves rotated by 38.2° relative to one another, and in combination they give the six pairs of spots. Similarly for the $(\sqrt{13}\times\sqrt{13})R13.9°$ reconstruction, there are two equally probable rotational domains, with the LEED patterns overlaid as shown in Fig. 5(b).

When the $(\sqrt{13}\times\sqrt{13})R13.9°$ and $(\sqrt{7}\times\sqrt{7})R19.1°$ LEED patterns are overlaid (effectively we have four overlaid patterns given that there are two rotational domains for each reconstruction) we obtain the pattern in Fig. 5(c). This has the "petal" structure already seen in the real LEED pattern shown in Fig. 5(d). The calculated [Fig. 5(c)] and experimentally observed [Fig. 5(d)] LEED patterns are equivalent, confirming the STM observation that both $(\sqrt{13}\times\sqrt{13})R13.9°$ and $(\sqrt{7}\times\sqrt{7})R19.1°$ reconstructions coexist on the surface.

C. Auger electron spectroscopy

Auger electron spectroscopy was carried out on a surface with the $(\sqrt{7}\times\sqrt{7})R19.1°$ and $(\sqrt{13}\times\sqrt{13})R13.9°$ coexisting reconstructions. This spectrum was compared to that of a sample that was cleaved in the UHV chamber, in order to achieve a surface that would be as close to $SrTiO_3$ stoichiometry as possible. Cleaving should produce a (100) interface (as that is the lowest-energy termination) with equal amounts of SrO and TiO_2 terminations.

Figure 6(a) shows the Auger spectrum obtained for the $(\sqrt{7}\times\sqrt{7})R19.1°$ and $(\sqrt{13}\times\sqrt{13})R13.9°$ co-reconstruction. The spectrum contains a featureless background, of relatively constant gradient, in the region 600–1400 eV. This featureless background, which was present in all Auger spectra from the $SrTiO_3$ surfaces, is thought to be independent of the nature of the surface, and is mainly dependent on the relative geometry between the sample, electron beam, and detector. It was hence assumed that the featureless background could be taken as a reference, and all spectra were scaled so that their featureless backgrounds overlapped. All spectra were normalized so that they had an intensity of 1000 counts at 1100 eV (a point in the featureless background).

Figure 6(b) shows a high-resolution scan of the $(\sqrt{7}\times\sqrt{7})R19.1°$-$(\sqrt{13}\times\sqrt{13})R13.9°$ coexisting reconstructions (black) and the cleaved sample (gray) between 350 and 550 eV. As indicated on the plot, the peaks at 380 and 413 eV (*LMM*) are due to the presence of Ti in the surface region. Similarly, the peaks at 492 and 511 eV (*KLL*) are characteristic of O. In an examination of the second Ti peak (at 413 eV) a shoulder can be seen on its right-hand side at slightly higher energy than the main peak. This is characteristic of Ti^{4+} species present in the surface. In contrast, if Ti^{2+} were present the shoulder would be on the opposite side. As the spectra have been normalized to the same reference point, we can subtract the cleaved spectrum from the $(\sqrt{7}\times\sqrt{7})R19.1°$-$(\sqrt{13}\times\sqrt{13})R13.9°$ spectrum, resulting in the graph in Fig. 6(c). In this difference plot, if a particular element has a positive peak (maximum), it indicates that the normalized peak for the $(\sqrt{7}\times\sqrt{7})R19.1°$-$(\sqrt{13}\times\sqrt{13})R13.9°$ surface was larger than that for the cleaved surface. Thus the species has a greater concentration in the $(\sqrt{7}\times\sqrt{7})R19.1°$-$(\sqrt{13}\times\sqrt{13})R13.9°$ reconstruction compared to a stoichiometric surface. Conversely, a negative dip (minimum) indicates a lower concentration of a species in the $(\sqrt{7}\times\sqrt{7})R19.1°$-$(\sqrt{13}\times\sqrt{13})R13.9°$ surface relative to stoichiometry. The plot shows that there is a greater Ti concentration in the $(\sqrt{7}\times\sqrt{7})R19.1°$-$(\sqrt{13}\times\sqrt{13})R13.9°$ sample compared to the stoichiometric cleaved sample. In addition the O concentration is lower in the $(\sqrt{7}\times\sqrt{7})R19.1°$-$(\sqrt{13}\times\sqrt{13})R13.9°$ sample relative to that of the stoichiometric surface.

Figure 6(d) shows high-resolution scans of the $(\sqrt{7}\times\sqrt{7})R19.1°$-$(\sqrt{13}\times\sqrt{13})R13.9°$ surface (black) and the cleaved surface (gray) in the energy range 1600–1800 eV. Sr is signified by peaks at 1644 and 1711 eV (*LMM*). Again

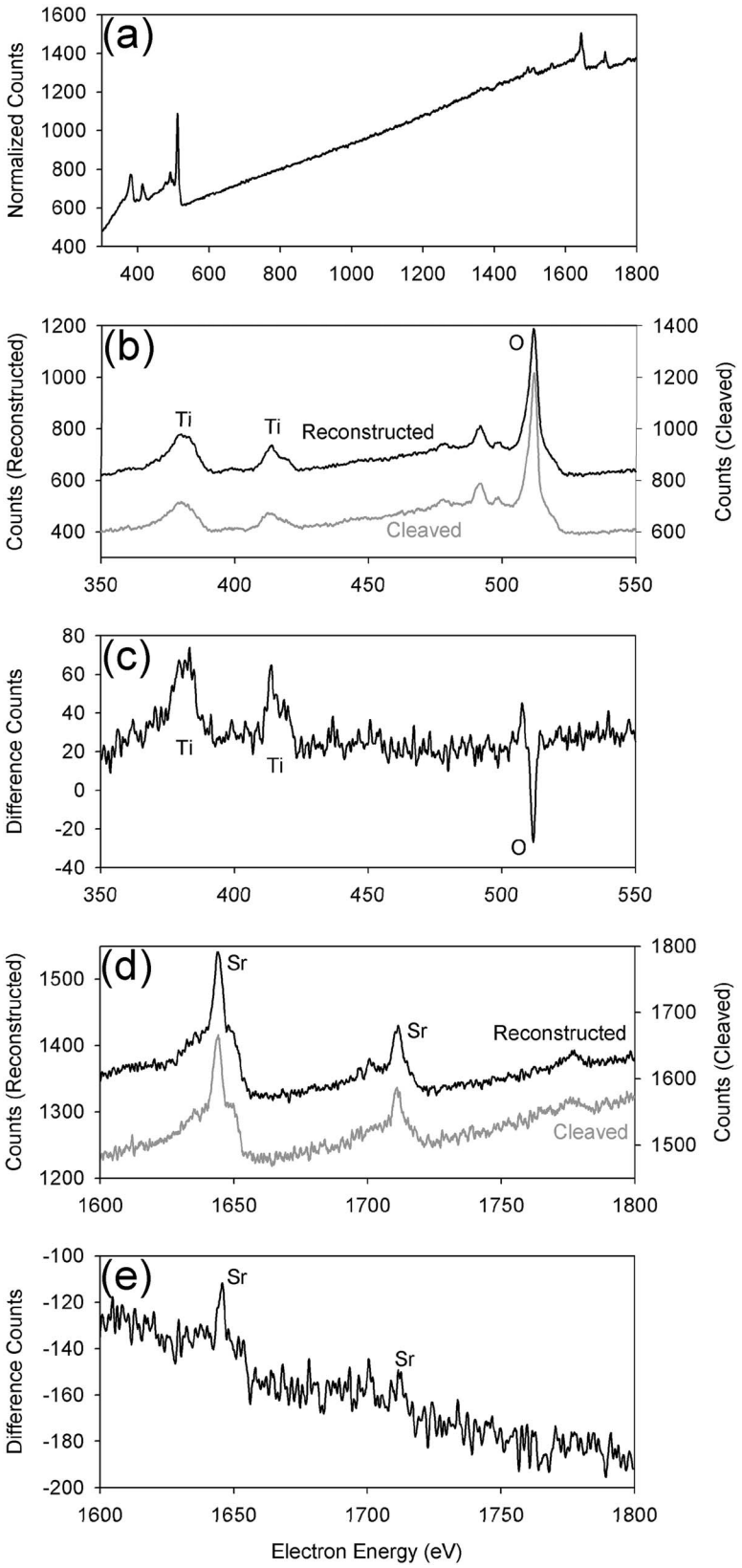

FIG. 6. (a) Auger spectrum from the $(\sqrt{7}\times\sqrt{7})R19.1°$-$(\sqrt{13}\times\sqrt{13})R13.9°$ surface. The spectrum has been normalized so that it has a value of 1000 counts at 1100 eV (a point within the featureless background). (b) High-resolution Auger spectra of the $(\sqrt{7}\times\sqrt{7})R19.1°$-$(\sqrt{13}\times\sqrt{13})R13.9°$ reconstruction (black) and a UHV cleaved surface (gray). This region shows the characteristic Ti [380 and 413 eV (*LMM*)] and O [492 and 511 eV (*KLL*)] peaks. (c) Difference plot for the cleaved spectrum in (b) subtracted from the $(\sqrt{7}\times\sqrt{7})R19.1°$-$(\sqrt{13}\times\sqrt{13})R13.9°$ spectrum in (b). Positive peaks indicate a greater concentration of a species in the $(\sqrt{7}\times\sqrt{7})R19.1°$-$(\sqrt{13}\times\sqrt{13})R13.9°$ surface compared with that of the stoichiometric cleaved surface. Negative dips indicate a lower concentration. The concentration of Ti in the $(\sqrt{7}\times\sqrt{7})R19.1°$-$(\sqrt{13}\times\sqrt{13})R13.9°$ surface is greater, and that of O is lower, in comparison to the stoichiometric cleaved surface. (d) High-resolution spectra of the $(\sqrt{7}\times\sqrt{7})R19.1°$-$(\sqrt{13}\times\sqrt{13})R13.9°$ (black) and cleaved (gray) surfaces. The Sr peaks are at 1644 and 1711 eV (*LMM*). (e) Difference plot for the cleaved spectrum in (d) subtracted from the $(\sqrt{7}\times\sqrt{7})R19.1°$-$(\sqrt{13}\times\sqrt{13})R13.9°$ spectrum in (d). A peak is present at 1644 eV, indicating a greater Sr concentration for $(\sqrt{7}\times\sqrt{7})R19.1°$-$(\sqrt{13}\times\sqrt{13})R13.9°$ relative to the cleaved sample.

we subtract the normalized spectrum for the cleaved data from that of the $(\sqrt{7}\times\sqrt{7})R19.1°$-$(\sqrt{13}\times\sqrt{13})R13.9°$ coexisting reconstruction, giving the plot in Fig. 6(e). This shows that the Sr level is larger in the $(\sqrt{7}\times\sqrt{7})R19.1°$-$(\sqrt{13}\times\sqrt{13})R13.9°$ surface compared to that of the stoichiometric cleaved surface.

By comparing the peak heights of the normalized spectra, the concentrations of Sr, Ti, and O are calculated. The nor-

malized peak heights for the cleaved spectrum were taken to indicate a stoichiometric surface, and so the relative Sr, Ti, and O concentrations were taken to be 1, 1, and 3, respectively. If the peak heights for the $(\sqrt{7}\times\sqrt{7})R19.1°$-$(\sqrt{13}\times\sqrt{13})R13.9°$ coexisting reconstruction are compared with those for the cleaved surface, we get Sr, Ti, and O concentrations of 1.16 ± 0.06, 1.31 ± 0.07, and 2.71 ± 0.04, respectively. This indicates an enrichment of the Sr concentration by 16%, and a Ti enrichment of 31%. The O, however, is deficient by 10%.

The starting point for the surface, however, is not stoichiometry. The surfaces of the samples, introduced to the chamber prior to annealing, are epi-polished. The AES spectra for these "as introduced" polished samples were also investigated. The obtained Sr, Ti, and O concentrations were 1.31 ± 0.07, 1.65 ± 0.07, and 2.60 ± 0.05. Compared with stoichiometry, this represents a Sr and Ti concentration enriched by 31% and 65%, respectively, and an O deficiency of 13%.

IV. DISCUSSION

STM and LEED indicate the presence of a $(\sqrt{7}\times\sqrt{7})R19.1°$-$(\sqrt{13}\times\sqrt{13})R13.9°$ co-reconstruction existing on the surface. Since these two reconstructions always coexist with significant quantities of each, it can be assumed that they are of similar surface energy. In addition, since they both form in the same conditions and from the same unsputtered, polished surface, it is also likely that they are of similar composition. The constant magnitude of the step heights allows the inference that steps have a height characteristic for the distance between two similar (111) planes, as the measured step heights are equivalent to the d_{111} lattice spacing. The haphazard shape of the domains suggests that each nucleates at a single point on the surface. The domain then grows until it meets another growing domain. This leaves a small region of disorder in the region separating the domains.

It was not possible to obtain more information per unit cell than that illustrated. The best STM images were obtained at relatively high bias, which usually has a detrimental effect on the amount of information in the picture. This only gives us one spot per unit cell which is not enough to start predicting the positions of atoms at the surface. As images were taken at positive bias (i.e., electrons tunneling from the tip into empty surface states) it is likely that they are dominated by Ti states, as these are the lowest-lying empty states above the Fermi level.[25] This cannot be stated conclusively, however, without knowledge of the surface structure and the aid of computer modeling.

The STM images are produced by electrons tunneling into or out of the surface, from or to the tip, respectively. If no states are present at the Fermi level, one would expect imaging to be impossible close to zero bias voltage, as there are no states available for electrons to tunnel between. On attempting to scan at a range of voltages, it was found that neither reconstruction could be imaged at sample voltages less than +1.0 V nor at negative bias. This shows that the surface states possess a band gap and are nonmetallic, with the Ti surface states pegged higher than 1 eV above the Fermi level. This property helps to indicate the Ti species present in the surface. TiO_2, which is an insulator, contains Ti^{4+}, whereas TiO and Ti_2O_3, both conductors at room temperature, are made up of Ti^{2+} and Ti^{3+}, ions, respectively. Hence, the surface must contain only Ti^{4+} and not Ti^{3+} or Ti^{2+} species, due to its nonmetallic nature. This was confirmed by the AES analysis, which showed the characteristic 414 eV peak for a Ti^{4+}-dominated sample.

As the two reconstructions coexist on the surface, and one must by necessity have a lower surface energy, this indicates that at least one must be a kinetic transition. However, we believe both reconstructions represent a kinetic phase on the $SrTiO_3$ (111) surface. On the (111) surface we have observed two families of reconstructions: the $(\sqrt{7}\times\sqrt{7})R19.1°$-$(\sqrt{13}\times\sqrt{13})R13.9°$ co-reconstruction and a family of $(n\times n)$ reconstructions which are formed after Ar ion sputtering. The AES results show that the $(\sqrt{7}\times\sqrt{7})R19.1°$-$(\sqrt{13}\times\sqrt{13})R13.9°$ and the as-introduced polished surfaces are both Sr enriched relative to stoichiometry. Neither of these surfaces were sputtered. Previous work on the $SrTiO_3$ (100) surface has shown that sputtering allows Ti to diffuse more easily to the surface, allowing the production of Ti-rich surface phases, and the expulsion of Sr from the surface region. On annealing sputtered $SrTiO_3$ (100), a number of nanostructures are formed on the surface[14–16] which have been shown to be Ti rich and formed from TiO_x. On the extreme end of the scale, anatase[26] can be formed on the surface of $SrTiO_3$ (100). As sputtering stimulates the ability of Ti to move to the surface region, it is likely that it will be the sputtered surfaces that will represent the thermodynamic minimum, as unsputtered surfaces are not given the opportunity to lower their energy via large-scale Ti diffusion. The $(\sqrt{7}\times\sqrt{7})R19.1°$-$(\sqrt{13}\times\sqrt{13})R13.9°$ surface is Sr enriched and, although it is less Sr and Ti enriched than the polished surface, it is likely that this is due to oxygen diffusion to the surface when the polished sample is annealed, rather than diffusion of the two other species. Therefore we believe that $(\sqrt{7}\times\sqrt{7})R19.1°$-$(\sqrt{13}\times\sqrt{13})R13.9°$ is a kinetic phase, as when Ti diffusion is also made available as a method of reducing the surface energy a different family of reconstructions is adopted.

As mentioned in the Introduction, there are four methods of removing the polarity: stoichiometry change at the surface, electron redistribution at the surface, adsorption of gaseous atoms or molecules, and faceting. There is no evidence of faceting in the images, and the AES spectra do not indicate any adsorption of foreign species. AES does show nonstoichiometry in the surface region, as Ti is enhanced and O is deficient. In order to confirm the driving force for the change in surface composition we compared the Auger spectrum of the reconstructed surface to that of an as-introduced polished sample. The polished sample had higher Sr and Ti concentrations (1.31 and 1.65, respectively) and lower O concentrations (2.60) than the reconstructed sample (Sr, 1.16; Ti, 1.31; O, 2.71). This shows that the annealing has significantly changed the surface composition from that of the as-introduced polished sample. As a result we can say that the reconstructed surface is not simply an ordering of the surface composition caused by the polishing process, but a

different structure which must be a response to the polarity of the $SrTiO_3$ (111) surface. The changes from the as-introduced composition to that of the reconstructed sample are an increase in O and a reduction in Sr and Ti. O can be mobile within $SrTiO_3$, and so it is likely that this is gained by O segregation from the bulk. This probably accounts for most of the changes in the concentrations of each species, as an increase in O will reciprocally cause a decrease in Sr and Ti concentration. However, as Sr and Ti have boiling points of 457 and 1207 °C at 10^{-8} Pa, it is possible that if Sr metallizes it can be removed by sublimation, but Ti cannot. Therefore it is possible that a small amount of Sr is lost via sublimation whereas some Ti may be lost via diffusion into the bulk. In addition, as both the Sr and Ti concentrations in the $(\sqrt{7}\times\sqrt{7})R19.1°$-$(\sqrt{13}\times\sqrt{13})R13.9°$ co-reconstruction are greater than those of a cleaved stoichiometric sample, it can be assumed that the surface is not made up of a pure TiO_x phase. Instead a phase with both Sr and Ti is present, but with Ti having a larger concentration. It is this phase, with its change in stoichiometry from that of the bulk, which neutralizes the macroscopic dipole and stabilizes the surface energy. As the surface is unsputtered, it is likely it will be kinetically unfavorable for a major reordering beyond the top few monolayers. This surface phase can clearly order in two different ways, with similar surface energies, giving rise to the two reconstructions observed.

It is also possible that the Nb doping may have an effect on the reconstructions. The Nb dopes *n*-type, inserting a small band of states just below the conduction band. This will alter the energy of the Fermi level. There is no evidence of Nb segregation from the bulk to the surface in the AES analysis. The Nb provides conduction electrons to the crystal. It is possible that these electrons could remove the polarity by distributing their charge in response to the polar electric field, and thus quenching it. This is possible because the electrons are in the conduction band and are thus able to freely arrange themselves in response to the field. This would have the effect of making particular reconstructions stable that would not be stable on the pure, undoped $SrTiO_3$ (111) surface. The $SrTiO_3$ (111) surface may, therefore, have different properties depending on whether it is doped or undoped.

V. CONCLUSIONS

On annealing in UHV at 850 °C for 30 min, Nb-doped $SrTiO_3$ (111) forms both $(\sqrt{7}\times\sqrt{7})R19.1°$ and $(\sqrt{13}\times\sqrt{13})R13.9°$ reconstructions which coexist on the surface. Both reconstructions are likely to be of similar energies. The top few monolayers are dominated by an ordered phase which is enriched in Ti and Sr, and deficient in O. This change in stoichiometry aids the removal of the dipole that would be present on bulk-terminated $SrTiO_3$ (111). On annealing, the surface is formed via the diffusion of O from the bulk to the surface of epi-polished samples, which are Sr and Ti enriched. The surface states have a band gap and the predominant Ti species is Ti^{4+}. The $(\sqrt{7}\times\sqrt{7})R19.1°$ and $(\sqrt{13}\times\sqrt{13})R13.9°$ reconstructions are most likely to be a kinetic phase of the $SrTiO_3$ (111) surface.

ACKNOWLEDGMENTS

The authors would like to thank D. T. Newell for allowing the reproduction of his UHV cleaved Auger data, L. D. Marks for his insightful comments and helpful suggestions, and Chris Spencer (JEOL U.K.) for his technical support. We are also grateful to the EPSRC and Royal Society for funding.

*Electronic address: martin.castell@materials.ox.ac.uk

[1] P. W. Tasker, J. Phys. C **12**, 4977 (1979).
[2] C. Noguera, J. Phys.: Condens. Matter **12**, R367 (2000).
[3] V. Agrawal, N. Chandrasekhar, Y. J. Zhang, V. S. Achutharaman, M. L. Mecartney, and A. M. Goldman, J. Vac. Sci. Technol. A **10**, 1531 (1992).
[4] J. G. Mavroides, J. A. Kafalas, and D. F. Kolesar, Appl. Phys. Lett. **28**, 241 (1976).
[5] S. Ferrer and G. A. Somorjai, Surf. Sci. **94**, 41 (1980).
[6] W. Menesklou, H. J. Schreiner, K. H. Hardtl, and E. Ivers-Tiffée, Sens. Actuators B **59**, 184 (1999).
[7] F. Silly and M. R. Castell, Appl. Phys. Lett. **87**, 063106 (2005).
[8] F. Silly and M. R. Castell, Appl. Phys. Lett. **87**, 213107 (2005).
[9] F. Silly and M. R. Castell, Phys. Rev. Lett. **94**, 046103 (2005).
[10] M. R. Castell, Surf. Sci. **505**, 1 (2002).
[11] N. Erdman, O. Warschkow, M. Asta, K. R. Poeppelmeier, D. E. Ellis, and L. D. Marks, J. Am. Chem. Soc. **125**, 10050 (2003).
[12] N. Erdman, K. R. Poeppelmeier, M. Asta, O. Warschkow, D. E. Ellis, and L. D. Marks, Nature (London) **419**, 55 (2002).
[13] T. Kubo and H. Nozoye, Phys. Rev. Lett. **86**, 1801 (2001).
[14] M. R. Castell, Surf. Sci. **516**, 33 (2002).
[15] H. L. Marsh, D. S. Deak, F. Silly, A. I. Kirkland, and M. R. Castell, Nanotechnology **17**, 3543 (2006).
[16] D. S. Deak, F. Silly, D. T. Newell, and M. R. Castell, J. Phys. Chem. B **110**, 9246 (2006).
[17] W. J. Lo and G. A. Somorjai, Phys. Rev. B **17**, 4942 (1978).
[18] Y. Haruyama, Y. Aiura, H. Bando, Y. Nishihara, and H. Kato, J. Electron Spectrosc. Relat. Phenom. **88-91**, 695 (1998).
[19] H. Tanaka and T. Kawai, Surf. Sci. **365**, 437 (1996).
[20] W. M. Sigmund, M. Rotov, Q. D. Jiang, J. Brunen, J. Zegenhagen, and F. Aldinger, Appl. Phys. A: Mater. Sci. Process. **64**, 219 (1997).
[21] S. Sekiguchi, M. Fujimoto, M. G. Kang, S. Koizumi, S. B. Cho, and J. Tanaka, Jpn. J. Appl. Phys., Part 1 **Part 1 37**, 4140 (1998).
[22] S. Sekiguchi, M. Fujimoto, M. Nomura, S. B. Cho, J. Tanaka, T. Nishihara, M. G. Kang, and H. H. Park, Solid State Ionics **108**, 73 (1998).
[23] O. Martin, A. M. Odlyzko, and S. Wolfram, Commun. Math. Phys. **93**, 219 (1984).
[24] J. A. Noland, Phys. Rev. **94**, 724 (1954).
[25] V. E. Henrich, G. Dresselhaus, and H. J. Zeiger, Phys. Rev. B **17**, 4908 (1978).
[26] F. Silly and M. R. Castell, Appl. Phys. Lett. **85**, 3223 (2004).
[27] K. Hermann, computer code LEEDPAT (Fritz-Haber-Institut, Berlin, 2006).